Geophys. J. Int. (2013) **194,** 1358–1373
Advance Access publication 2013 June 18
doi: 10.1093/gji/ggt213

Integrated geophysical modelling of a lateral transition zone in the lithospheric mantle under Norway and Sweden

Sofie Gradmann,[1] Jörg Ebbing[1,2] and Javier Fullea[3,4]

[1]*Geological Survey of Norway, Trondheim, Norway. E-mail: Sofie.Gradmann@NGU.NO*
[2]*Department of Petroleum Engineering and Applied Geophysics, NTNU, Trondheim, Norway*
[3]*Institute of Geosciences, CSIC-UCM, Madrid, Spain*
[4]*Dublin Institute for Advanced Studies, Dublin, Ireland*

Accepted 2013 May 21. Received 2013 May 15; in original form 2012 November 2

SUMMARY

The Scandinavian Mountain Chain (the Scandes) exhibits characteristics that are unusual for an old, Palaeozoic mountain belt. These include renewed Neogene uplift in a passive margin setting and the lack of a pronounced crustal root. We investigate the influence of present-day thermal, compositional and geometric structures in the crust and mantle on the topography of the southern Scandes and the resulting implications for the tectonic history of Fennoscandia.

A self-consistent 3-D subsurface model of southern Norway and Sweden is constructed from recent geophysical data sets that constrain the crustal architecture, lithosphere geometry, density distributions and thermal properties. Recent seismological studies show evidence for a relatively abrupt transition from seismically slower lithospheric mantle underneath southern Norway to seismically faster lithospheric mantle underneath southern Sweden.

We find that a transition from thin subcontinental lithospheric mantle (SCLM) underneath southern Norway to a significantly thicker SCLM beneath southern Sweden can explain this velocity trend. A difference in composition between the two SCLM domains (owing to different depletion/refertilization) is required to satisfy the gravity field and isostatically compensated topography, but contributes only slightly to the observed velocity contrast. Such a lateral transition zone, constituting a major change in the lithospheric structure in southwestern Fennoscandia, can be related to several major Proterozoic and Phanerozoic tectonic events such as the Sveconorwegian orogeny, the Permian Oslo Rift and perhaps even the opening of the Atlantic.

Key words: Gravity anomalies and Earth structure; Composition of the mantle; Dynamics of lithosphere and mantle; Dynamics: gravity and tectonics; Mechanics, theory and modelling.

1 INTRODUCTION

The Scandinavian Mountain Chain (the Scandes) extends along the western margin of Fennoscandia covering nearly all of Norway and parts of northern Sweden (Fig. 1a). Between two domains of relatively high elevation (>500 m), termed northern and southern Scandes, more subdued topography is found in the intermediate region of central Norway. The mountain chain largely coincides with the extent of the Caledonian nappes, the remnants of the Caledonian orogen (Fig. 1b).

The elevated masses of orogenic belts formed during continent–continent collision are commonly isostatically supported by a crustal root. The Moho beneath the Scandes (Fig. 2a), however, does not exhibit a distinct crustal root but a gradual deepening towards the Fennoscandian shield in the east (e.g. Kinck *et al.* 1993; Grad *et al.* 2009). A local rise of the Moho is observed under the region of the Oslo Graben, resulting in a small root-like structure under the southern Scandes (Stratford *et al.* 2009). In the north, only the eastward Moho deepening is observed, but no crustal root is present. Nevertheless, a Bouguer anomaly low coincides with the elevated regions (Fig. 2b), indicating a high degree of isostatic compensation of the topography in the entire area (Balling 1980). The apparent inconsistency in northern Norway between the lack of a crustal root and the isostatic compensation is resolved from isostatic modelling by a high-density lower crustal layer (LCL) that extends east of the Scandes and thickens with decreasing topography (Ebbing 2007; Ebbing *et al.* 2012). Its presence has been seismically documented in eastern Fennoscandia (Lund 1987; Guggisberg *et al.* 1991; Korsman *et al.* 1999) and under central Norway (England & Ebbing 2012).

Several regional and global tomographic studies indicate a low-velocity anomaly in the upper mantle under southern Norway (Husebye *et al.* 1986; Bannister *et al.* 1991; Pilidou *et al.* 2004; Weidle & Maupin 2008; Schivardi & Morelli 2009), though the resolution is often coarse and the anomaly remains poorly constrained. A recent study of *P*-wave residuals reveals large differences in seismic velocities across a narrow belt between southern Sweden and

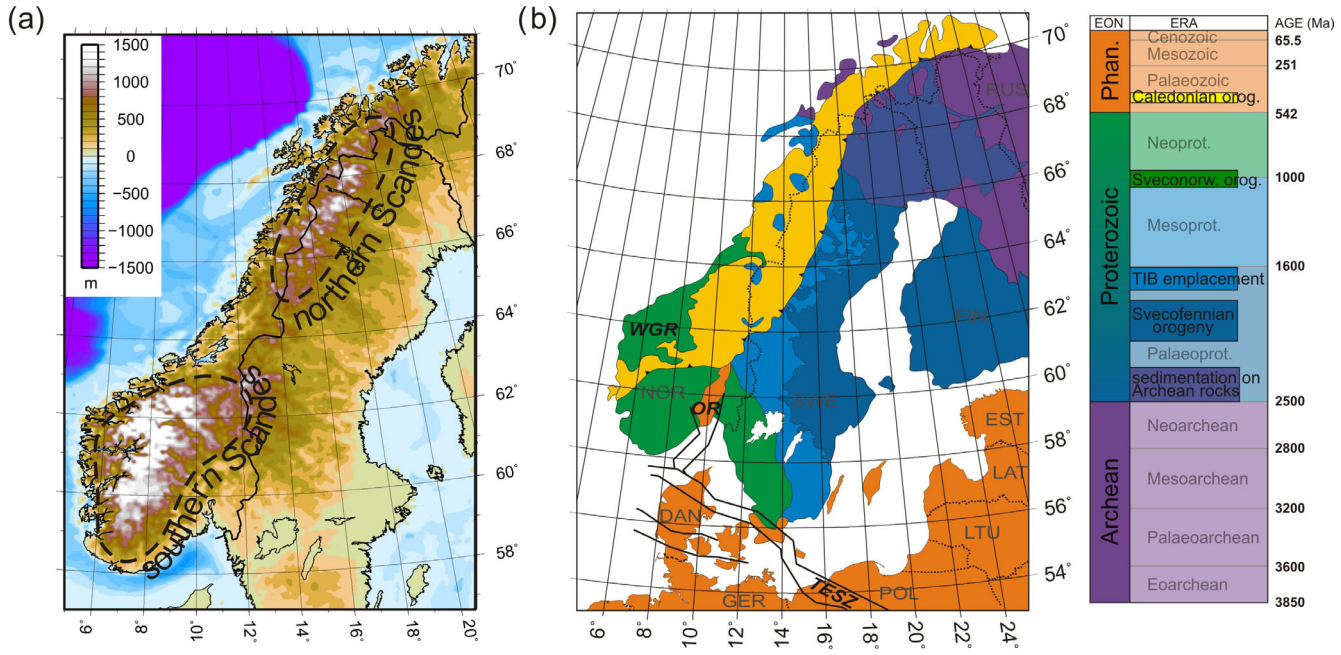

Figure 1. (a) Topography of western Fennoscandia with indicated division into southern and northern Scandes. (b) Simplified geological map of northern Europe and geological timescale showing relevant Fennoscandian tectonic events; WGR, Western Gneiss Region; OR, Oslo Rift; TESZ, Trans-European Suture Zone; TIB, Transscandinavian Igneous Belt (modified after Gorbatchev 2004; Eken *et al.* 2008).

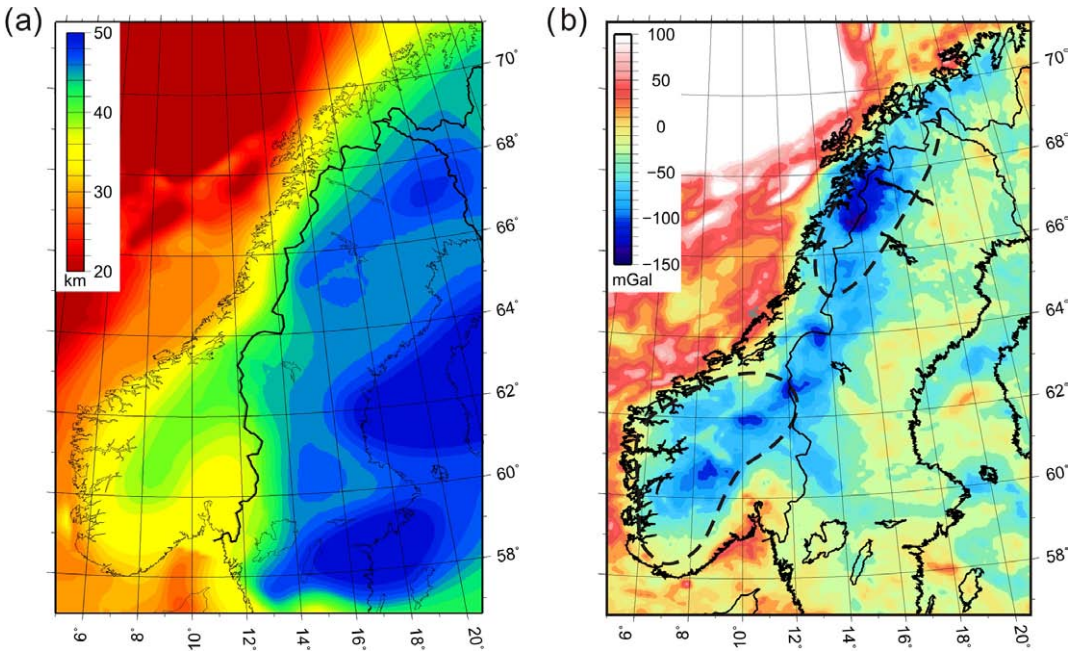

Figure 2. (a) Moho depth of western Fennoscandia, compiled from Kinck *et al.* (1993) and Stratford *et al.* (2009). Whereas a minor crustal root can be interpreted under southern Norway, a gradual eastward deepening of the Moho is seen for northern Norway. (b) Bouguer anomaly of western Fennoscandia (Andersen *et al.* 2010).

southern Norway and Denmark (Fig. 3a, Medhus *et al.* 2009, 2012). A similar pattern is seen in *S*-wave tomography (Wawerzinek *et al.* 2013). Velocity–depth profiles obtained from inversion of surface waves dispersion curves (Fig. 3b) confirm a large velocity contrast between seismic velocities underneath southern Sweden and southern Norway and Denmark (Cotte *et al.* 2002; Maupin 2011).

The above observations show that the simple model of a homogenous crust overlying a uniform mantle is too simplistic to represent the structure of western Fennoscandia. Lateral variations in structure and density of the crust and the underlying lithospheric mantle have large effects on the regional gravity field and the isostatic compensation (Ebbing 2007; Kolstrup *et al.* 2012). In this part of the study we employ several new and old geophysical data sets from southwestern Fennoscandia to constrain a self-consistent 3-D subsurface model. We focus in particular on the new models of Moho depth and seismic mantle velocities (Maupin *et al.* 2013), as well as the geological interpretation and implications of the modelled lithospheric structures.

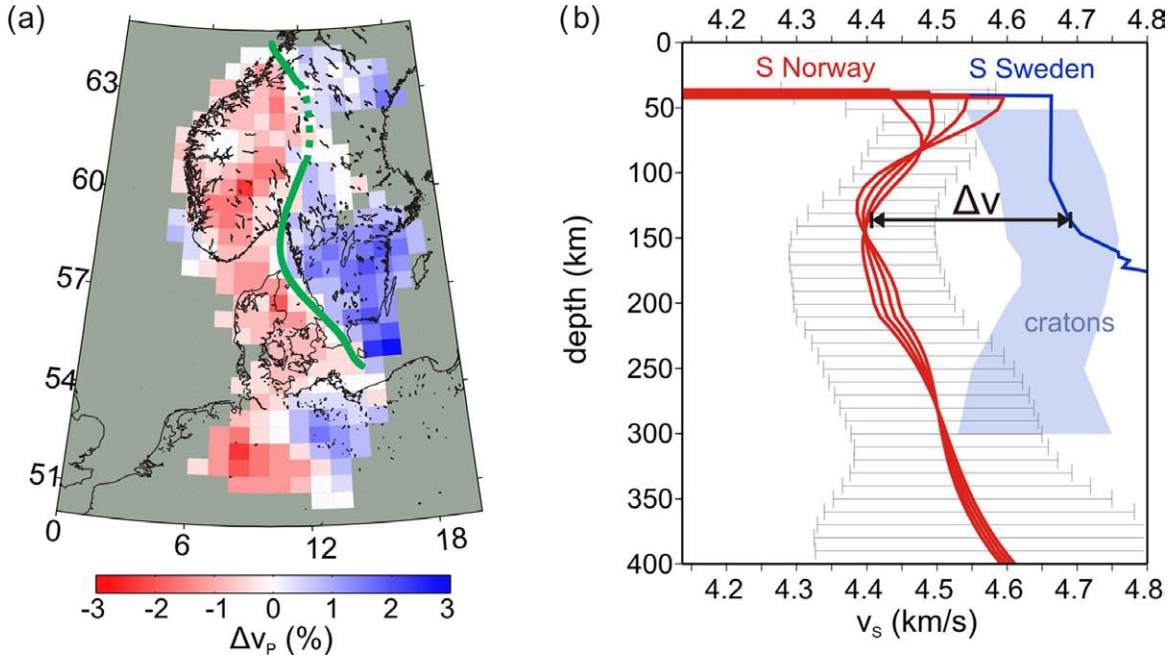

Figure 3. Results of teleseismic surveys from western Fennoscandia. (a) Regional *P*-wave tomography at 100–200 km depth. Green line indicates suggested lithospheric transition zone. From Medhus *et al.* (2012). (b) *S*-wave velocity with depth from southern Norway (red curves from Maupin 2011), southern Sweden (dark blue line from Cotte *et al.* 2002) and other Archean and Palaeoproterozoic cratons (blue area from Pedersen *et al.* 2009). Velocity–depth curves are derived from inversion of surface wave data; different Moho depth estimates lead to different seismic velocities of the subcrustal lithosphere (Maupin 2011).

1.1 Geological background: history of western Fennoscandia

Fennoscandia constitutes the westernmost part of the East European craton and encompasses crustal domains of Archean, Proterozoic and Phanerozoic tectonothermal ages (Fig. 1b). The Archean craton extends across northern Finland and northern Sweden (Gaal & Gorbatschev 1987; Lahtinen *et al.* 2005). The Palaeoproterozoic crust of southern Finland and Sweden was formed by terrane accretion and arc magmatism during the Svecofennian orogeny (2.1–1.8 Ga ago, Gorbatschev & Bogdanova 1993; Bingen *et al.* 2005; Lahtinen *et al.* 2005). At the end of the orogeny (1.86–1.65 Ga ago), the Transscandinavian Igneous Belt (TIB) was emplaced at the edge of the Svecofennian domain (Patchett *et al.* 1987; Gorbatschev & Bogdanova 1993). TIB is a collective term for a *ca.* 1400 km long, roughly north–south trending batholith belt, partly covered by Caledonian rocks. Three age groups have been identified (Larson & Berglund 1992; Åhäll & Larson 2000; Gorbatchev 2004) with an overall westward younging trend. Emplacement mechanisms suggested for the TIB vary from a continent-scale eastward subduction zone (e.g. Åhäll & Larson 2000; Lahtinen *et al.* 2009) to an extensional intracontinental setting (Korja *et al.* 1993; Anderson 1997).

The terranes of the Sveconorwegian Province (also called Southwest Scandinavian Domain) were formed and modified during one or multiple orogenic events. During the Gothian orogeny (1.75–1.55 Ga) the terranes of southwestern Sweden, mainly east of the Oslo Rift, were accreted onto the Svecofennian domain (Åhäll & Larson 2000), yet the existence of this orogenic phase is debated (Andersson *et al.* 2002). The entire Sveconorwegian region was reworked during the Sveconorwegian-Grenvillian orogeny (1.14–0.9 Ga, e.g. Gorbatschev & Bogdanova 1993; Bingen *et al.* 2005), when additional terranes of today's southern Norway were accreted. It is not clear whether the Sveconorwegian orogeny accreted allochthonous terranes or re-organized existing terranes (Bingen *et al.* 2008). Strongest deformation occurred in the region around and to the west of today's Oslo Graben, diminishing towards the north.

During the Caledonian orogeny (440–410 Ma) collisions with Laurentia in the west and Avalonia in the south affected the margin of Baltica. Allochthonous nappes of the Caledonides are still overlying the Proterozoic basement in Norway and Sweden, and form the bulk part of the Scandinavian Mountain Chain (the Scandes). Along the southern margin of Baltica, orogenic remnants are no longer present, but crustal and upper-mantle structures reveal a major scar, the Trans-European Suture Zone (TESZ; Arlitt *et al.* 1999; Cotte *et al.* 2002; Plomerová *et al.* 2002; Shomali *et al.* 2002, 2006).

The Caledonian Mountains were lowered during orogenic collapse soon after collision and a number of additional extensional phases followed since. During the Permian, the Oslo Rift formed as a localized extensional feature with minor magmatic activity. Widespread extension during the Late Jurassic to Early Cretaceous caused substantial thinning of the crust in today's shelf areas (Færseth & Lien 2002; Osmundsen *et al.* 2002; Osmundsen & Ebbing 2008). Rifting of the pre-thinned crust during the Palaeogene led to the break-up of the Atlantic Ocean and was the last tectonic event in the western Fennoscandian region.

There are several lines of evidence indicating one or more phases of post-rift uplift of the Norwegian Margin, encompassing offshore unconformities (Japsen *et al.* 2007), geomorphologic studies (Lidmar-Bergström *et al.* 2000, 2007; Osmundsen & Redfield 2011; Redfield & Osmundsen 2012), and thermochronological data (Redfield *et al.* 2005; Japsen *et al.* 2012). The mechanisms that could have led to post-rift uplift along the passive margin of Norway are debated and range from influence of the Iceland plume and mantle upwelling to intraplate stresses or dynamic topography (Doré *et al.* 2002; Anell *et al.* 2009; Esedo *et al.* 2012). An alternative explanation assigns the profound changes in erosion and exhumation history to climatic conditions and isostatic response, thereby negating any

tectonic uplift component (Nielsen *et al.* 2009). With this study, we aim to improve the constraints on the suggested mantle processes by better classifying and understanding the deep lithospheric structure.

2 INTEGRATED GEOPHYSICAL-PETROLOGICAL MODELLING

2.1 Method: LitMod3D

In this study, we model the lithospheric structure using the integrated geophysical modelling software LitMod3D (Afonso *et al.* 2008; Fullea *et al.* 2009). LitMod3D integrates geophysical and petrological forward modelling of the lithosphere and the sublithospheric mantle shallower than the transition zone within a self-consistent thermodynamic framework. By solving the appropriate heat transfer, thermodynamical, rheological, geopotential and isostasy equations, key physical properties in the mantle (e.g. seismic velocities, density and electrical conductivity) are determined as a function of pressure, temperature and bulk composition. We iteratively estimate the 3-D density and temperature distributions within the model domain before computing geophysical observables such as the geoid, surface heat flow, gravity anomalies, and isostatically adjusted topography. Our approach generates thermodynamically self-consistent 3-D subsurface models that can simultaneously account for a large number of geophysical and petrological observables, thus significantly reducing the uncertainties associated with modelling these data sets separately or in pairs. The methodology and finite-element code for the 2-D version (LitMod) are described in detail in Afonso *et al.* (2008), and extension of this methodology to 3-D modelling is described in Fullea *et al.* (2009). Here we give an overview of the main aspects of the method, strategies and assumptions involved, in particular those relevant to our study. The modelling workflow is presented in Fig. 4.

The models comprise crust, lithospheric mantle and sublithospheric mantle down to a depth of 400 km. The lithosphere–asthenosphere boundary (LAB) separates the outermost, cold and relatively rigid layer of the Earth (lithosphere) from the warmer and rheologically weaker sublithospheric or asthenospheric mantle. The base of the lithosphere is marked by a change in different physical parameters and processes, for example, strain rate, heat transfer mechanism, seismic velocity, electric conductivity, seismic anisotropy, etc. (Eaton *et al.* 2009; Fischer *et al.* 2010; Yuan & Romanowicz 2010, and references therein). The term 'lithosphere' is used in this study primarily as a synonym of the thermal lithosphere. The latter is defined as the 'cold' outermost layer of the Earth, in which heat transfer is dominated by conduction (e.g. Schubert *et al.* 2001). Hence, in this work we adopt a thermal definition of the LAB, allowing at the same time compositional variations within the lithospheric mantle.

The base of the lithosphere is simultaneously defined as the 1315°C isotherm and a compositional boundary. In the lithosphere, the temperature distribution is calculated by solving the 3-D steady-state heat conduction equation using a P-T-dependent thermal conductivity (Afonso *et al.* 2008; Fullea *et al.* 2009) and considering a set of appropriate boundary conditions. In the sublithospheric mantle the heat transport is dominated by convection and therefore, the geotherm is assumed to follow here an adiabatic gradient (e.g. Afonso *et al.* 2008). A zone in which both convection and conduction take place connects the two domains (i.e. the base of the thermal lithosphere and the adiabatic mantle). This superadiabatic zone of variable thickness mimics the thermal effect of a rheologically active layer at the base of the upper thermal boundary layer in the convecting mantle (Solomatov & Moresi 2000; Zaranek & Parmentier 2004).

Each crustal layer in LitMod is characterized by its thermal properties and density. The lithospheric and sublithospheric mantle materials are primarily characterized by their distinct major-element bulk compositions in the CFMAS scheme (CaO–FeO–MgO–Al_2O_3–SiO_2). Additionally, empirical parameters that control the pressure and temperature dependency of the thermal conductivity are required. These have been determined in laboratory experiments (Hofmeister 1999).

Stable mineral phases at given pressure–temperature conditions in the mantle are calculated using a scheme based on the minimization of Gibbs free energy within the major oxide system CFMAS (Connolly 2005). To avoid the spurious effect of small proportions of extra oxides commonly present in xenolith-derived mantle

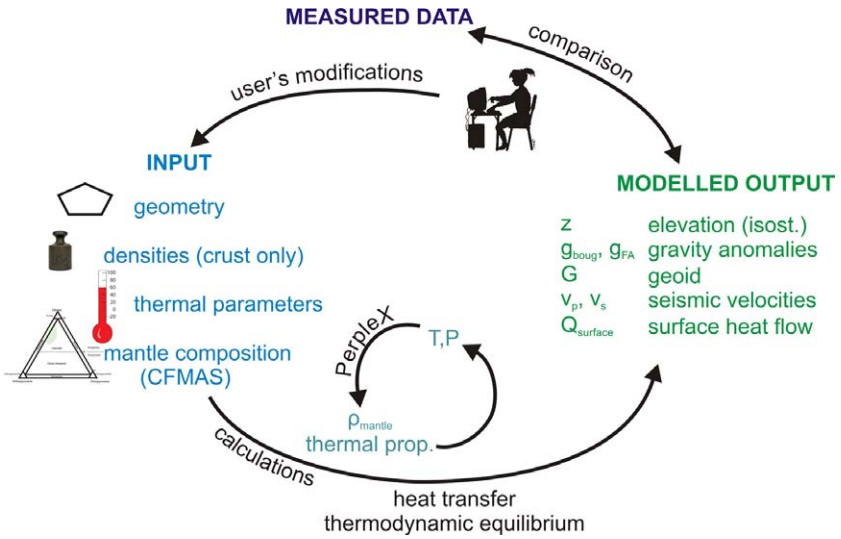

Figure 4. Simplified flow chart of LitMod3D.

Table 1. Data sets used to constrain the preliminary model.

Data set	Region	Reference
Model geometry		
Elevation/bathymetry	Global	Scripps/NOAA data set, Smith & Sandwell (1997)
Basement/sediment thickness	Norwegian Margin/global	Ebbing & Olesen (2010), NOAA data set, Divins (2012)
Intracrustal layers	Southern Norway	Stratford *et al.* (2009)
Moho depth	Fennoscandia	Compilation, Grad *et al.* (2009); Kinck *et al.* (1993); Stratford *et al.* (2009)
Thickness of lower crustal layer	Western Fennosandia	Ebbing (2007)
Base lithosphere	Fennoscandia	Calcagnile (1982)
Geophysical observables		
Elevation/bathymetry	Global	Scripps/NOAA data set Smith & Sandwell (1997)
Bouguer gravity	Global	DTU2010, Andersen *et al.* (2010)
Free-air gravity	Global	DTU2010, Andersen *et al.* (2010)
Geoid	Global	EGM08, Pavlis *et al.* (2008)

compositions (i.e. outside the CFMAS system) we recast the amounts of the five oxides for them to add up to 100 per cent prior to computing the Gibbs free energy minimization. The bulk rock properties are averaged from the stable mineral phases. Seismic velocities in the mantle are determined according to the elastic moduli of each end-member mineral and the density of the bulk rock, as described by Connolly & Kerrick (2002).

Geoid and gravity anomalies are calculated by adding the individual contributions of a number of rectangular, flat-topped prisms of either constant or linearly varying density (Nagy *et al.* 2000; Fullea 2008). Gravity anomalies are shifted by a constant value in order to obtain a best match with the observed data and minimize the residuals. The geoid is corrected with a constant tilt, eliminating long-wavelength signals. The reader is referred to Fullea *et al.* (2009) for more technical details about how these geophysical observables are computed. The isostatically balanced elevation is based on the pressure distribution at the base of the model and is calculated with respect to a reference lithospheric column (Afonso *et al.* 2008). Flexural isostasy is obtained by calling an external finite-difference program (TISC Garcia-Castellanos 2002), which requires the 2-D load distribution and a representative effective elastic thickness for the lithosphere. The flexural load is given by pressure variations at the compensation level.

Seismic anelasticity is considered a posteriori in the calculations by including attenuation effects on seismic mantle velocities. These are calculated as a function of grain size d, oscillation period T_0, temperature T, pressure P, activation energy E, activation volume V and empirical parameters A and α (e.g. Minster & Anderson 1981; Karato 1993; Afonso *et al.* 2005)

$$v = v_0(T, P)\left[1 - \frac{1}{2}\cot\left(\frac{\pi\alpha}{2}\right) Q^{-1}\right] \tag{1}$$

$$Q_s^{-1} = A\left\{\frac{T_0}{d}\exp\left[\frac{-(E + VP)}{RT}\right]\right\}^{\alpha} \tag{2}$$

$$Q_p^{-1} = \frac{4}{9}Q_s^{-1}, \tag{3}$$

where v and v_0 are the attenuated and non-attenuated P- or S-wave velocities, Q_s and Q_p are the respective quality factors and R is the universal gas constant.

2.2 Input data

2.2.1 Geometry

A number of data sets are used to geometrically define the 3-D subsurface starting model (Table 1). Modifications to this starting model are discussed with the introduction of the models of Fennoscandia (Section 3).

The topography is taken from the Scripps/NOAA global data set (Smith & Sandwell 1997). The offshore sedimentary thickness is derived from the top basement map of Norway and its continental shelf (Ebbing & Olesen 2010) and extended with the NOAA global sediment thickness data set (Divins 2012). The internal crustal structure in southern Norway shows a very uniform layering with near-constant depth to the top and base of the middle crust, not following the trend of the Moho depth (Stratford *et al.* 2009). For simplicity, this layering has been expanded further to the east and north across the model domain. A thinning of the middle crust has been introduced towards the offshore regions. Depth and thickness of the LCL (lower crustal layer) are taken from the isostasy modelling of Ebbing (2007). Various Moho depth maps covering northern Europe have been published in the past decades (Kinck *et al.* 1993; Grad *et al.* 2009). Additionally, regional studies of Moho depths have been conducted for southern Norway (Svenningsen *et al.* 2007; Stratford *et al.* 2009). We use a compilation by Ebbing *et al.* (2012) of the most recent data sets, which provide the smallest and best-constrained uncertainties.

The LAB marks a region at the base of the lithosphere where a number of physical parameters change (rheology, heat transfer mechanism, seismic velocity, electric conductivity, seismic anisotropy, etc.). The depth of this boundary (or layer) therefore depends on which physical parameters are mapped and which geophysical methods are used. Compilations of LAB depths under western Fennoscandia comprise teleseismic measurements (Calcagnile 1982; Plomerová *et al.* 2008), heat flow calculations (Artemieva *et al.* 2006) and local magnetotelluric measurements (Korja *et al.* 2008; Jones *et al.* 2010). The LAB of our starting model stems from the data set of Calcagnile (1982), but is considered poorly constrained.

2.2.2 Crustal thermophysical properties

The crustal densities (Table 2) are chosen according to previous gravity studies and surface rock measurements (Ebbing *et al.* 2012, and references therein). The origin of high-density, high-velocity

Table 2. Modelling properties of crustal material.

Layer	Density, ρ (kg m^{-3})	Thermal conductivity, k [W (m K)$^{-1}$]	Heat production rate, A (μW m^{-3})
Shallow sediment	2335	2.5	2
Deep sediment	2550	2.5	2
TIB	2700	2.4	2
Upper crust (west)	2750	2.4	2
Upper crust (east)	2800	2.4	2
Middle crust (west)	2850	2.4	0.5
Middle crust (east)	2900	2.4	0.5
Lower crust (west)	2950	2.0	0.4
Lower crust (east)	2990	2.0	0.4
Lower crustal layer (LCL)	3180	2.0	0.4

lowermost crust is debated and explanations range from eclogized crust to subducted oceanic crust and mafic underplating (Korsman *et al.* 1999; Cook *et al.* 2010). Our high LCL model density (3180 kg m^{-3}) is consistent with an eclogitic nature of the lower crustal layer but not contradicting other origins. We here take the view that the modelled LCL mainly reflects the strong density increase with depth in thick continental crust, but do not propose a particular origin.

Mantle densities are derived based on the major-element compositions, temperature and pressure as described in Section 2.1. Heat production in the crust decreases with depth, values of 1–2.7 μW m^{-3} have been derived from thermal modelling for the upper crust (Kolstrup *et al.* 2012), of 0.6–3 μW m^{-3} from geochemical analysis of surface rocks (Olesen *et al.* 2007; Slagstad 2008). The values chosen for this study fall into this range of data (2.0 μW m^{-3} for sediments and upper crust, 0.5 μW m^{-3} for middle and lower crust). Thermal conductivities are described by a value of 2.5 W (m K)$^{-1}$ for the upper, 2.0 W (m K)$^{-1}$ for the lower crust (Slagstad *et al.* 2009; Kolstrup *et al.* 2012).

2.2.3 Mantle composition and thermophysical properties

Mantle composition generally varies with the grade of depletion and therefore with the age of the lithospheric mantle. As a rule of thumb, Archean lithospheric mantle has the highest magnesium and lowest iron content with an average magnesium number of 92.7 (Mg# $= 100 \times$ Mg/(Mg + Fe), values in molar per cent) and lowest bulk densities; Phanerozoic lithospheric mantle has lower magnesium and higher iron content (Mg# ∼89.9) and higher bulk densities (e.g. Djomani *et al.* 2001; Grad *et al.* 2009). We use average compositions based on the tectono-thermal age of the mantle terranes (Phanerozoic, Proterozoic and sublithospheric) as compiled by Afonso *et al.* (2008; Table 3). The choice of compositions for the different models is discussed in Section 3.1. The mantle compositions are defined in terms of the weight percentages of the five most abundant oxides (CFMAS system). These oxides are the main constituents of the most common upper-mantle minerals (olivine, orthopyroxene, clinopyroxene, spinel, garnet, pyroxene, ringwoodite and wadsleyite; Stixrude & Lithgow-Bertelloni 2005). Other elements constitute only minor parts (*ca*. 1 per cent) of the bulk mantle composition, yet their influence can be significant in some physical properties like seismic velocities and electric conductivities.

The crust of southern Norway (our main study area) formed during the Proterozoic Sveconorwegian orogeny. Archean-type mantle is exposed in parts of the Western Gneiss Region in Western Norway (Beyer *et al.* 2004). However, multiple tectonic events affected and likely heated and refertilized the lithospheric mantle during the Phanerozoic (Caledonian orogeny, formation of Oslo Rift, Late-Mesozoic rifting, opening of the Atlantic). We therefore choose a Phanerozoic-type subcontinental lithospheric mantle (SCLM) composition for our starting model ***Scand1***. We later investigate a Proterozoic-type composition for the older, Palaeoproterozoic areas of the model domain.

The thermophysical properties of the stable mineral assemblages are calculated using the set of parameters given in Table 3. These

Table 3. Modelling properties of mantle materials. Mantle composition taken from Afonso *et al.* (2008).

	Symbol	Unit	Phanerozoic mantle	Proterozoic mantle	Sublithospheric mantle
Thermal parameters					
Heat production rate	A	μW m^{-3}	0.01	0.001	0.0
Thermal expansion coefficient	α		0.31×10^{-4}	0.31×10^{-4}	0.3×10^{-4}
Reference thermal conductivity	k_0	W (m K)$^{-1}$	5.3	4.5	0.0
Grüneisen parameter	γ		125	125	–
Isothermal bulk modulus	K_T	GPa	4.3	4.3	–
K_T pressure derivative dK_T/dP	K_0		130	130	–
Composition					
SiO_2		per cent	44.5	44.6	45.0
Al_2O_3		per cent	3.5	1.9	4.5
FeO		per cent	8.0	7.9	8.1
MgO		per cent	39.8	42.6	37.8
CaO		per cent	3.1	1.7	3.6
Mg#			89.9	90.6	89.3

empirical parameters refer to the bulk rock for a generic SCLM rather than to the individual minerals, because the uncertainty of the controlling parameters yields variations in thermal conductivity that are of the same order as the compositional dependence. The values for the two different SCLM bulk compositions used in this study (Phanerozoic-type and Proterozoic-type) are chosen from the range of reasonable values such that the differences in seismic velocities are maximized, which is of importance for this study, as discussed later.

2.2.4 Geophysical observables

A number of geophysical data sets are used for comparison of the modelled observables. The geoid is taken from EGM2008 (Pavlis *et al.* 2008) with removal of the low-wavelengths of spherical harmonic order and degree lesser than ten. Bouguer and Free-Air anomalies are taken from the DTU2010 data set (Andersen *et al.* 2010). Bouguer reduction densities are 2670 and 1670 kg m^{-3} for onshore and offshore areas, respectively.

Regional tomographic data sets often have a too coarse resolution to resolve the lithospheric structures of southwestern Fennoscandia. Local tomographic studies have been performed in southern Norway (Medhus *et al.* 2012; Wawerzinek *et al.* 2013). Velocity–depth profiles (Fig. 3b) have been determined for the same area by Maupin (2011) and for southern Sweden and Denmark by Cotte *et al.* (2002).

A regional heat flow data set of Norway has been compiled by Slagstad *et al.* (2009). However, these data are strongly influenced by local anomalies and can therefore only provide a rough guideline to the regional modelling and are not specifically considered in this study.

3 MODELLING RESULTS

Here we present the results of two different 3-D subsurface models. The geometry of model ***Scand1*** mainly reflects the existing data sets as described in Section 2. Modifications to this geometry comprise adjustments to the thickness of the LCL (in onshore and offshore regions), but are minor. Model ***Scand2*** is a variation of model ***Scand1*** with primary changes in the composition and thickness of the lithospheric mantle. Additional differences between the two models concern the crustal densities and thickness of the LCL, as described below.

3.1 Model *Scand1*: prototype

Design of model ***Scand1***

Model ***Scand1*** is mainly built on the existing data sets described in Section 2. The model domain comprises southern Norway and southern Sweden up to 65°N (Figs 5a and b) and is split into 72 × 72 × 203 cells, yielding a depth resolution of 2 km, a N–S resolution of *ca.* 14 km, and an E–W resolution between 12 and 15 km, depending on latitude.

A vertical cross section at 61°N (Fig. 5c) shows the sediments, the three-layered crust, the TIB, the LCL and the lithospheric and sublithospheric mantle. Uniform crustal layering, as evident from southern Norway (Stratford *et al.* 2009), is extrapolated to the adjacent regions. This simplified geometry does not do justice to the offshore areas, where basement highs, small-scale sedimentary basins, lower crustal bodies and basalt flows result in locally complex patterns (Olesen *et al.* 2010). Because the focus of this paper is the deep lithospheric structure of (mainly onshore) southwestern Fennoscandia and the vertical model resolution is only 2 km, we retain a simplified offshore crustal structure and fit gravity and elevation data allowing moderate changes in the sediment thickness and Moho depth. This simplified offshore structure precludes detailed geodynamic interpretations there. However, including this first-order structure minimizes any bias due to offshore misfits in onshore model estimates.

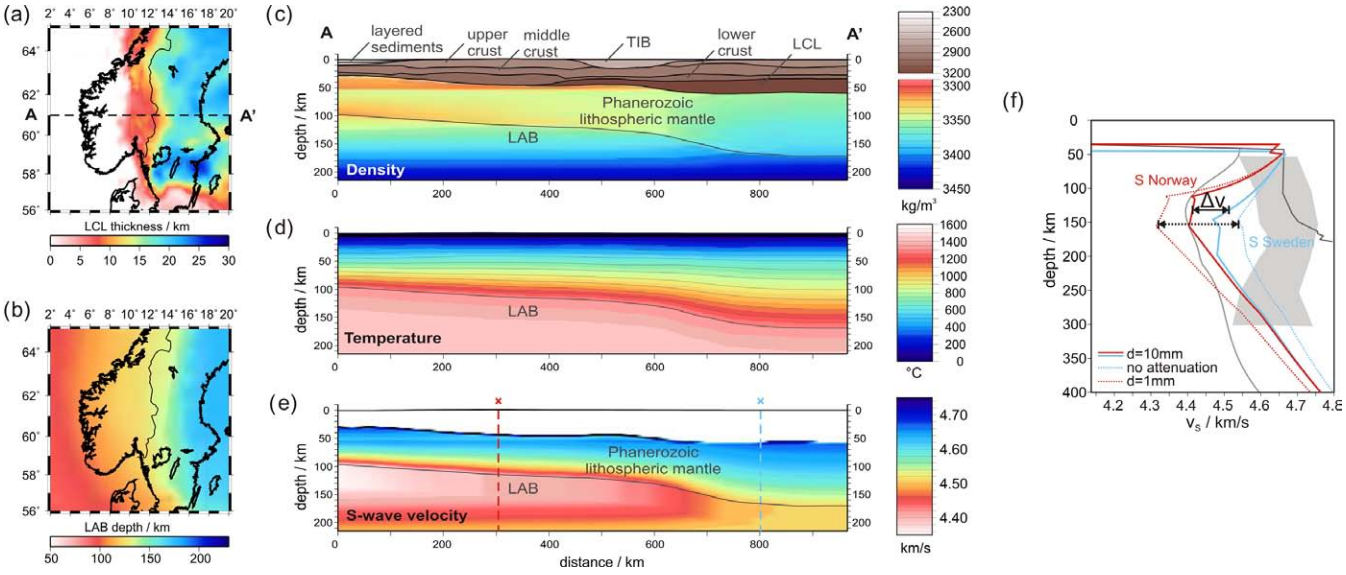

Figure 5. (a) Thickness of lower crustal layer in model ***Scand1***. (b) Depth to lithosphere–asthenosphere boundary (LAB) in model ***Scand1*** (from Calcagnile 1982). (c) Cross section at 61°N showing the subsurface model geometry and density distribution. TIB, Transscandinavian Igneous Belt; LCL, lower crustal layer. (d) Temperature of model ***Scand1*** along cross section at 61°N. (e) *S*-wave velocity of model ***Scand1*** along cross section at 61°N showing an overall velocity increase to the east. (f) Comparison of measured (grey) and modelled (red, blue) velocities of southern Norway and southern Sweden. Locations of velocity–depth profiles are shown in (e). Modelled velocity differences between these regions are *ca.* 0.1 km s^{-1}. Velocity differences similar to observed ones can be obtained with somewhat unrealistic attenuation factors equivalent to very small grain size, *d*, under Norway paired with infinite grain size (no attenuation) under Sweden.

The upper boundary of the high-density lower crustal layer is modified in order to obtain a best fit with the observed gravity and elevation data (Fig. 5a). The lower boundary of the LCL (the Moho) is kept fixed throughout the model area. For model ***Scand1***, the depth of the LAB is taken from Calcagnile (1982, Fig. 5b). The lithospheric mantle has a homogenous, Phanerozoic composition.

Results of model ***Scand1***

The calculated isostatically compensated elevation, Bouguer gravity and geoid agree fairly well with the measured data (Fig. 6). A belt of positive elevation residuals stretches north–south around 14°E (Fig. 6g), correlating with the LAB depth used in the model (Fig. 5b). Without modifying Moho or LAB depth, we were not able to eliminate this residual, which is a first indicator that the used input data sets do not represent the deep lithospheric structures correctly. Differences in elevation are generally <150 m in the onshore areas, slightly larger residuals remain offshore (Fig. 6g). Differences in gravity are less than 15 mGal and differences in geoid height less than 1.5 m.

An E–W cross section of seismic velocities of the lithospheric and sublithospheric mantle shows an overall increase towards the east, mimicking the density and temperature trend (Figs 5c–e). This is a direct effect of the lithosphere thickness: the deeper the 1315°C isotherm, the colder the lithospheric mantle, the higher the seismic velocities. A comparison to velocity–depth profiles from southern

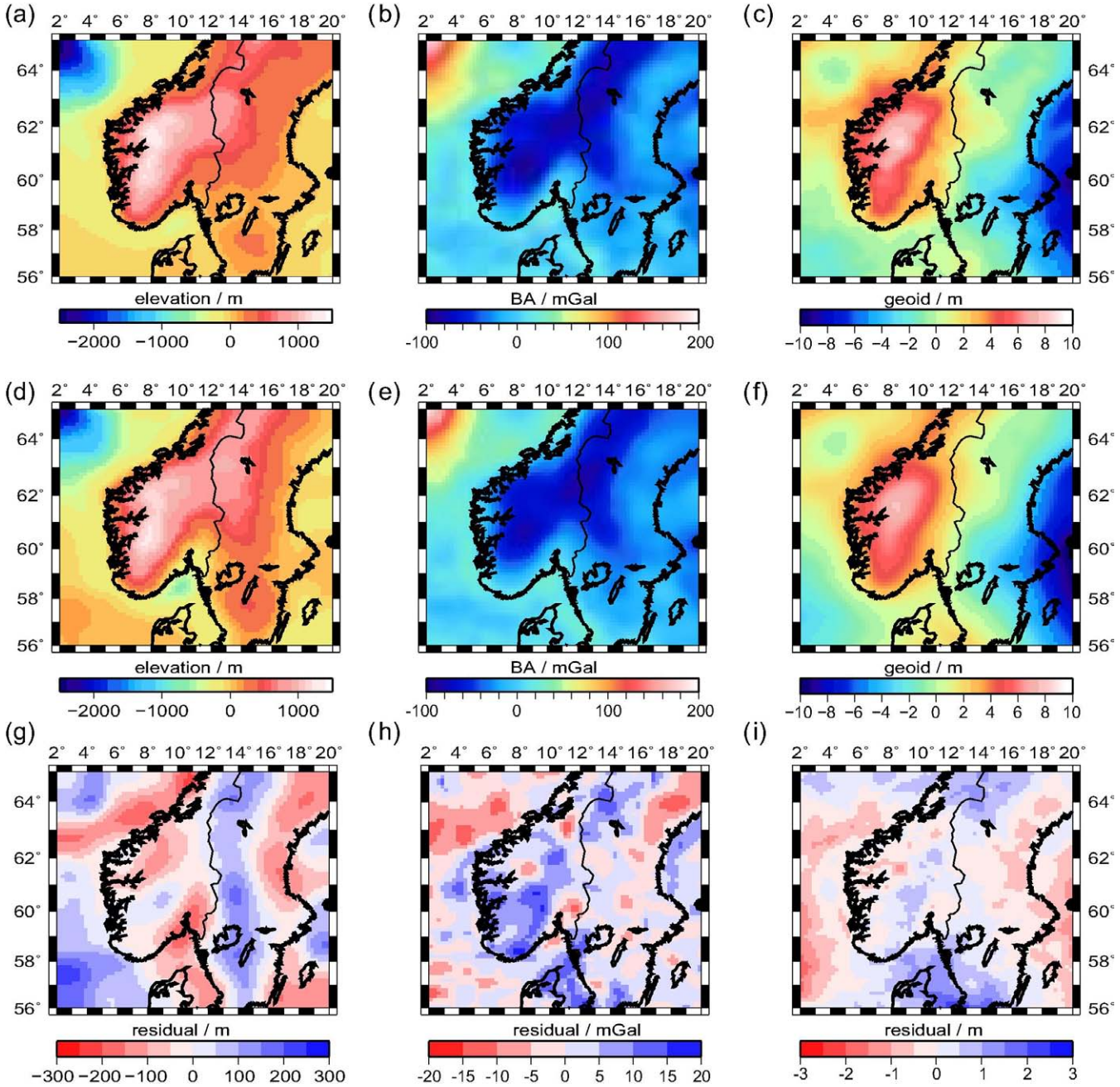

Figure 6. Isostatically compensated elevation, Bouguer gravity and geoid (degree and order $n \geq 11$) of southwestern Fennoscandia (a–c) and from model ***Scand1*** (d–f). Panels (g–i) show the respective residuals (difference between modelled and observed values).

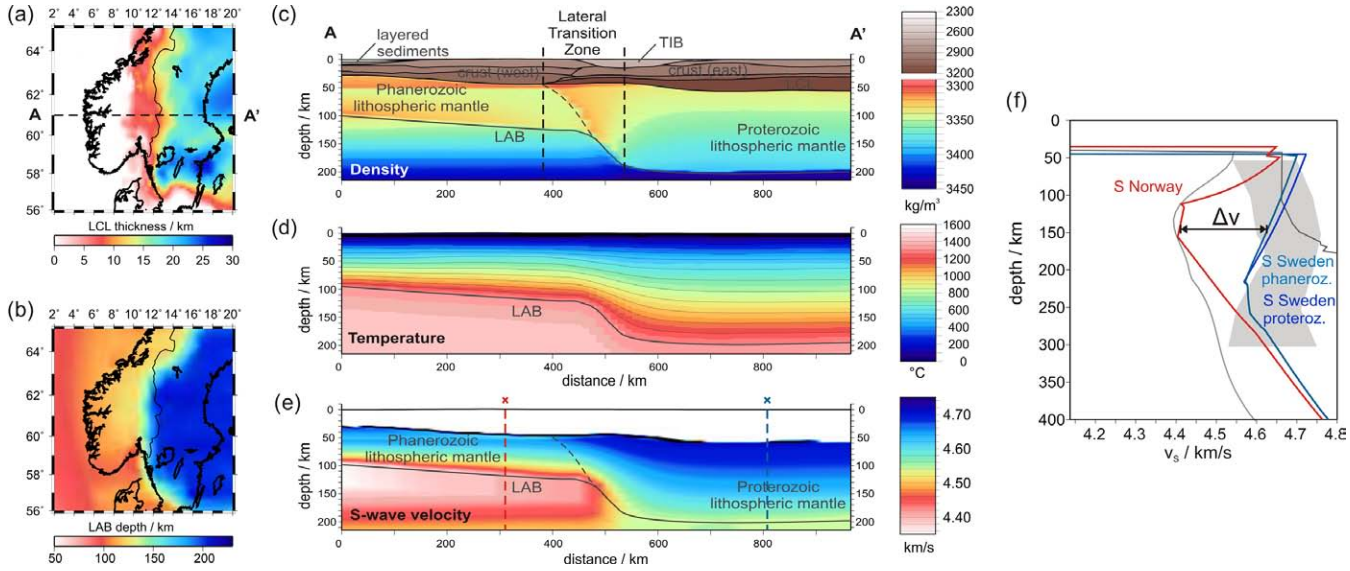

Figure 7. (a) Thickness of lower crustal layer in model ***Scand2***. (b) Depth to lithosphere–asthenosphere boundary (LAB) in model ***Scand2***. (c) Cross section at 61°N showing the subsurface model geometry and density distribution. Difference to model ***Scand1*** are the depth of the LAB, the Proterozoic composition of the eastern subcontinental lithospheric mantle (SCLM) and higher densities in the eastern crust. TIB, Transscandinavian Igneous Belt; LCL, lower crustal layer. (d) Temperature of model ***Scand2*** along cross section at 61°N. (e) *S*-wave velocity of model ***Scand2*** along cross section at 61°N showing an overall velocity increase to the east. (f) Comparison of measured (grey) and modelled (red, blue) velocities of southern Norway and southern Sweden. Calculations with Phanerozoic mantle composition of the thick, eastern lithosphere indicate that compositional differences only lead to minor velocity changes.

Norway and southern Sweden (Fig. 5f, solid lines) shows that modelled velocity differences between these two regions are less than 0.1 km s^{-1} and thus substantially smaller than the >0.2 km s^{-1} velocity difference observed in seismological data (Fig. 3b).

One explanation for this larger velocity difference could be different attenuation in both regions. Among the different factors that influence attenuation (pressure, temperature, oscillation period, etc.), grain size is the one that may vary strongest among different lithospheric regions and thus provides the largest net effects. Tests with different attenuation factors (Fig. 5f, dashed lines) show that only a relatively small grain size of 1 mm under southern Norway paired with an infinite grain size under southern Sweden (equivalent to no attenuation) can lead to velocity differences similar to those observed. These values are nevertheless unrealistic and furthermore, the absolute velocity values do not match the observed ones. Model ***Scand1*** is thus not capable of explaining the lithospheric velocity structure, although it fits the elevation and gravity data.

3.2 Model *Scand2*: lithospheric step

Design of model ***Scand2***

In order to model high seismic velocities such as observed under southern Sweden (Cotte *et al.* 2002; Maupin *et al.* 2013), the LAB (1315°C isotherm) of model ***Scand2*** is significantly deepened to *ca.* 200 km under Palaeoproterozoic southern Sweden (Fig. 7b). Furthermore, the thermophysical parameters are varied slightly within the range of empirical values to yield a yet colder SCLM. In addition to the thermal thickness of the SCLM, its composition is also modified to match Proterozoic-type SCLM (Table 3). A thicker, colder lithosphere reduces the buoyancy in comparison to the thinner lithosphere of model ***Scand1***. A more depleted mantle composition, which yields lower average densities, is necessary to counteract this effect. Slightly higher crustal densities are chosen for the Palaeoproterozoic domains (Fig. 7c and Table 2). LCL thickness is again modified in order to best fit the observed gravity and elevation data (Fig. 7a).

We refer to the change from thinner, more fertile SCLM to thicker, colder and more depleted SCLM as a lateral transition zone (Fig. 7c). It is not to be confused with the (vertical) mantle transition zone at 410 km depth.

Results of model ***Scand2***

The isostatically compensated elevation, Bouguer gravity and geoid heights by which model ***Scand2*** is constrained, are shown in Fig. 8. The peak amplitudes of the residuals are identical to those for model ***Scand1***(Figs 8g–i). However, we observe a spatially better fit to data compared to model ***Scand1***, with the residuals no longer correlating with the LAB depth.

The cross section of seismic velocities (Fig. 7e) shows, as expected, a much larger increase of seismic velocities and decrease of temperatures towards the east than in model ***Scand1***. Temperatures in the SCLM are up to 300°C different between the two models. The comparison of velocity–depth profiles to the observed velocities (Fig. 7f) shows a much better fit, both with respect to the difference between velocities under southern Norway and Sweden and with respect to the absolute values.

A model similar to model ***Scand2***, but with Phanerozoic mantle composition yet without renewed adjustment of geometry and densities, yields only a marginally lower seismic velocity (Fig. 7f, medium blue line). This demonstrates that the mantle composition does not have a large effect on seismic velocities in these models, where only five major elements are considered and that the large velocity differences between model ***Scand1*** and ***Scand2*** are almost exclusively temperature effects.

4 DISCUSSION

Both models ***Scand1*** and ***Scand2*** yield similar topography and gravity signals but differ fundamentally in the velocity structure

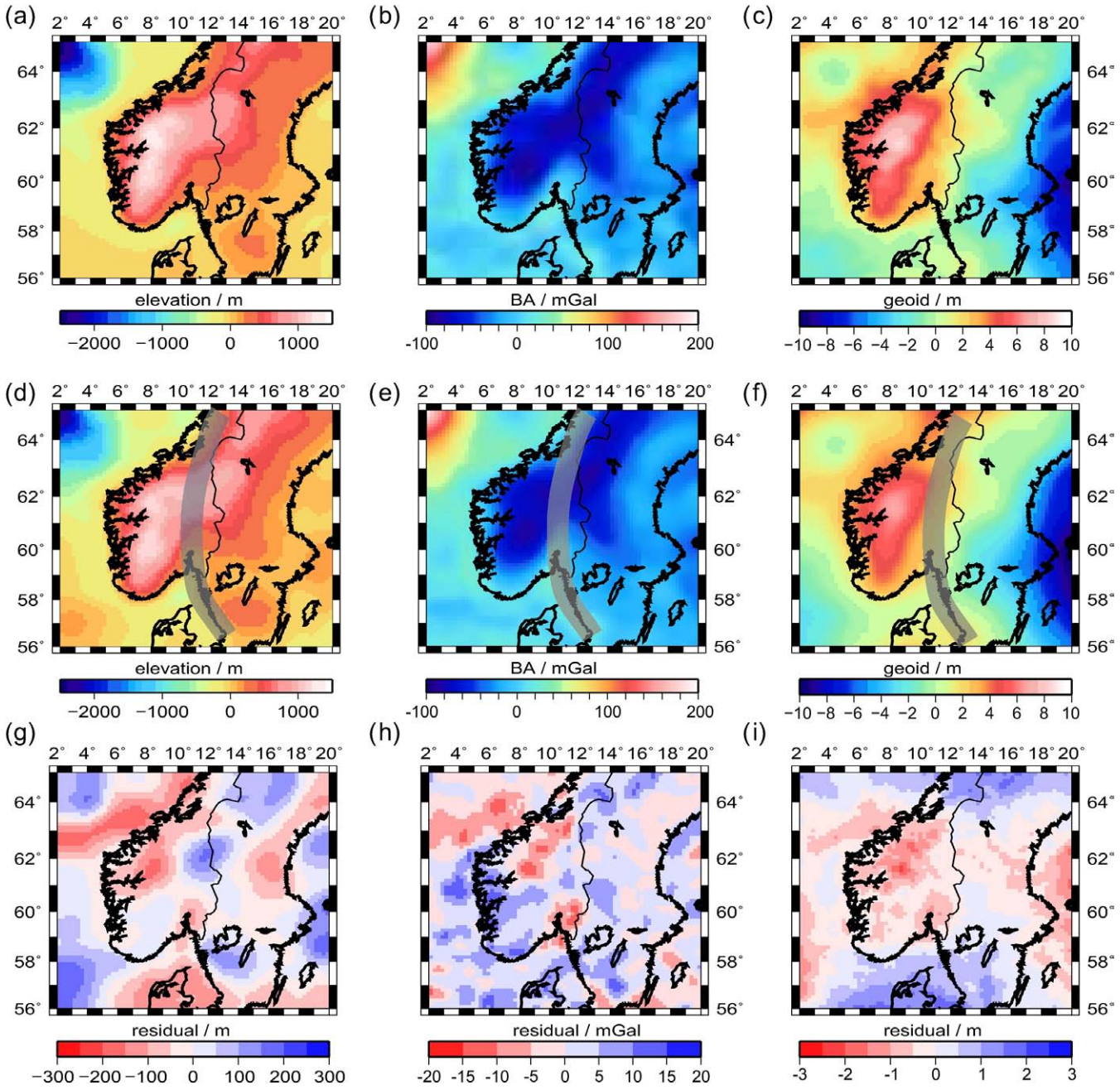

Figure 8. Isostatically compensated elevation, Bouguer gravity and geoid (degree and order $n \geq 11$) of southwestern Fennoscandia (a–c) and from model ***Scand2*** (d–f). Grey line marks the location of the lateral lithospheric transition zone. Panels (g–i) show the difference between the modelled and the observed values.

of the uppermost mantle. We here discuss these differences with respect to the measured seismic velocities and with respect to the region's tectonic history.

4.1 The velocity structure

The models of Section 3 demonstrate that an abrupt change in lithosphere depth and hence in temperature towards Sweden can explain the observed lateral velocity changes. The velocity structure with depth is, however, not properly reproduced by the models. Although the calculated absolute and relative velocities in depth of 100–150 km fit quite well with the measured data, large discrepancies remain between the calculated and measured velocities of the shallow sublithospheric and shallow lithospheric mantle of southern Norway, as well as for the overall velocity trend in the lithospheric mantle under southern Sweden.

Fig. 3 shows that the Moho depth assumed for the inversion from surface wave data significantly affects the sub-Moho velocities. However, in our forward model, very high sub-Moho velocities are calculated independently of Moho depths (see Figs 5e and f). The forward calculated velocities are based on a model which assumes thermal equilibrium and no compositional layering of the mantle (hence no additional changes in elastic moduli and thermal properties), and is therefore oversimplified.

We need to conclude that our models cannot properly reproduce the actual velocity–depth profiles. However, where the velocity

differences between domains of different lithosphere thickness are largest (120–150 km depth), the agreement of modelled and measured velocities is acceptable. We consider it therefore justified to use the seismic velocities at this depth to constrain the LAB depth of the subsurface model. Its position is thus relatively well constrained in central Norway and southwestern Sweden, but much more poorly in the continuation to the north and south. In the overall picture, however, model ***Scand2*** provides a reasonably good fit to the seismic velocity data from cratonic areas as well as to the topography and gravity signal. As discussed above, first-order compositional differences and changes in grain size have a comparatively small effect on the seismic velocities of the modelled SCLM and thus can explain only a small part of the velocity difference. However, only five major oxides are considered in the models (i.e. CFMAS system) and additional oxides may change the seismic velocity gradient. For example, chromium oxide strongly affects the depth of the spinel-garnet phase change and thus the velocities below 50 km (Klemme 2004; Lebedev *et al.* 2009), in particular in cratons with relatively Cr-rich compositions. Compositional differences also implicate changes in thermal properties, which can in extreme cases lead to velocity differences of up to 2.5 per cent (Hieronymus & Goes 2010). In the models, the thermophysical properties of the SCLMs are already adjusted to minimize temperature in the Proterozoic mantle, and hence maximize the seismic velocities. High water content, which is considered to decrease seismic velocities significantly (Popp & Kern 1993; Karato & Jung 1998), is commonly only found above subduction zones—a setting that has not been present in our study area for approximately one billion years.

Temperature variations may stem from thermal anomalies in addition to the modelled differences in tectonothermal age and lithosphere thickness. An anomalously hot mantle under southern Norway has been proposed previously, either as the result of a finger of hot mantle from Iceland (Weidle & Maupin 2008) or in combination with a sublithospheric diapir (Rohrman & van der Beek 1996). The latter interpretation has often been debated and recently been rejected (e.g. Pascal & Olesen 2009). The hypotheses of an anomalously hot Norwegian mantle could indeed explain large velocity differences, but would result in absolute velocities much lower than the observed ones. Furthermore, very thin lithosphere under southern Norway is not consistent with the low to moderate heat flow values measured here (Slagstad *et al.* 2009).

4.2 A major suture zone beneath southern Norway and Sweden?

The models of Section 3 favour an abrupt change in lithosphere thickness between southern Norway and southern Sweden, which is also consistent with earlier regional seismological studies (Plomerová *et al.* 2001, 2008). Several other instances of relatively abrupt changes in the LAB structure have been revealed in the last decade by high-resolution geophysical imaging of the uppermost mantle (Cotte *et al.* 2002; Babuška & Plomerová 2004; Petit & Déverchère 2006; Medhus *et al.* 2009, 2012). These observations are independent of whether the LAB is mapped as a seismic, thermal or compositional boundary, and have mainly been interpreted as changes in lithosphere thickness. The best-studied example of a lithospheric step is the Trans-European Suture Zone, the southern edge of the Baltic Shield (Fig. 1b). From northern Germany into Sweden, an increase in lithospheric thickness from less than 100 km to nearly 200 km has been documented (Cotte *et al.* 2002; Shomali *et al.* 2002; Babuška & Plomerová 2004). The origin of this structure is related to its role as a suture zone between Proterozoic Baltica and Phanerozoic Europe, and represents a feature that has been involved in multiple Phanerozoic events. If the proposed lithospheric step beneath southern Norway and Sweden was to mark a similar juxtaposition of two very different lithospheric mantle domains, it would equally represent an old, but very significant suture zone.

The longevity of abrupt thickness changes of the lithosphere is puzzling, because both convective erosion and diffusion of the lateral temperature gradient would tend to smooth out the step. However, one possibility supported by geodynamic modelling is that lithospheric steps can survive for several hundreds of millions of years if a large viscosity contrast exists between the lithospheric and sublithospheric mantle, which could be attributed to compositional differences (Hieronymus *et al.* 2007).

The proposed lithospheric step or mantle boundary coincides largely with the location of the Oslo Graben (*ca.* 300 Ma), the location of the main deformation during the Sveconorwegian orogeny (0.9–1.1 Ga), the approximate location of the TIB in the northern part of the model domain (1.7 Ga) and the westward pinch-out of the LCL. The enormous time span that is bridged by these geological features can hardly be explained by a single process, but can indicate that major lithospheric structures are reactivated during subsequent geological processes or, even more, that they may serve as nuclei for renewed tectonic deformation.

A very interesting instance of this phenomenon has been demonstrated by numerical thermomechanical modelling of the deformation and temperature evolution during the Permian extension in southwestern Fennoscandia (Pascal *et al.* 2004). In this region of the Oslo Rift, field observations document substantial but very localized deformation and magmatism (Neumann *et al.* 1992). The study concludes that a pre-existing step in the lithosphere of several tens of kilometres was required to focus deformation west of the Oslo Rift. Steps of less than 50 km can indeed localize thermal anomalies (Pascal *et al.* 2002) but either lead to significant thinning of the eastern (thicker) domain or yield very wide-spread deformation, both inconsistent with observations of magmatism and geological structures (Pascal *et al.* 2004).

Such a step-like feature must accordingly have existed prior to the Permian formation of the Oslo Rift. The main part of the Caledonian orogeny occurred west of the Oslo Rift and is therefore considered unlikely to have created such a step-like structure in the lithosphere. The proposed feature is, however, consistent with several characteristics of the Sveconorwegian orogeny. The growth of Baltica by the accretion of the southern Norwegian terranes occurred during the late Meso- and early Neoproterozoic along the zone that later hosted the Oslo Rift. However, the eastern front of the Sveconorwegian deformation is not marked by the Oslo Rift but further to the east by the Mylonite Zone in southern Sweden, which is also considered an older terrane boundary (Åhäll & Larson 2000), distinguishing the Palaeoproterozoic TIB and the Idefjorden terrane of Gothian age (1.64–1.52 Ga). Magmatic activity and ductile deformation was more abundant and long-lived in the western part of the Sveconorwegian domain suggesting that this area was relatively warm (e.g. owing to a thinner lithosphere). It is not resolved whether the Sveconorwegian orogeny marks the accretion of allochthonous terranes onto Baltica or a redistribution of the Baltic crust. The second interpretation is not consistent with a western lithosphere that was thin prior to or thinning during the Sveconorwegian orogeny.

Only north of the Oslo Rift is the lateral transition zone located at the edge of the Svecofennian domain, which is generally marked by the TIB. Its different location in the southern part of the model domain may be a consequence of the multiple tectonic events that

affected the region. Neither the Sveconorwegian orogeny nor the earlier tectonic events (e.g. Gothian orogeny) are currently satisfactorily understood (Åhäll & Larson 2000; Andersson *et al.* 2002; Slagstad *et al.* 2013). Nevertheless, a variety of evidence from geological observations point towards a long-lived suture zone at the western edge of the Baltic shield (proximity of the edge of the Svecofennian domain, the TIB as the product of a major subduction zone, the main deformation of the Sveconorwegian orogeny and location of the Oslo Rift). Such a suture would not only show a geological near-surface expression but would include significant variations in physical properties with depth. Hence, such a mantle boundary may be located or distributed over a different area than the geological boundary at the surface. In the following section we discuss the potential effects of such a major SCLM suture zone on geophysical observables, and the implications for the western edge of the Baltic Shield.

4.3 Effects of laterally varying mantle characteristics

Lateral changes of SCLM properties in model ***Scand2*** (Section 3.2) affect not only seismic velocities, but also the gravity field and the isostatic compensation. These effects are difficult to address in the complex models shown in Section 3, as they are additionally affected by changes in Moho depth and LCL thickness. We therefore show simplified, laterally uniform (quasi-2D) models with a homogenous crust in order to quantify the effects of lateral variation of the different SCLM parameters.

Synthetic models

All of the four synthetic models shown in Fig. 9 (named ***Syn******) comprise a uniformly thick crust of 35 km underlain by a sublithospheric mantle with a step-like increase in thickness from 65 to 115 km.

This step is either smooth (***-sm***) or sharp (***-sh***), paired with either only Phanerozoic (***-PhPh***) or Phanerozoic-Proterozoic SCLM (***-PhPr***). The combination of step smoothness and mantle composition results in four end member models: ***Syn-sm-PhPh***, ***Syn-sh-PhPh***, ***Syn-sm-PhPr***and ***Syn-sh-PhPr***. The remaining model parameters are as those of models ***Scand1*** and ***Scand2*** and as listed in Tables 2 and 3.

Models ***Syn-sm-PhPh*** and ***Syn-sh-PhPh*** with uniform lithospheric mantle composition (Figs 9c and g) show a shift in the regional gravity signal and the isostatically balanced topography across the lithospheric step (light grey lines in Figs 9a, b, e and f). This is a simple effect of the mass difference between the warmer and lighter thin lithosphere and the colder and denser thicker lithosphere. These large regional shift (150 mGal, 1500 m) are in nature generally counterbalanced by changes in crustal thickness. In the case of southwestern Fennoscandia, an eastward deepening Moho and thickening LCL are concurrent with the deepening of the LAB.

Models ***Syn-sm-PhPr*** and ***Syn-sh-PhPr*** with laterally varying lithospheric composition (Figs 9d and h) show smaller changes of background levels of the Bouguer anomaly and isostatically compensated topography (40 mGal and *ca.* 400 m, respectively). This indicates that long-wavelength gravity signals (e.g. 20 mGal for Fennoscandia) can be rooted in the uppermost mantle. The synthetic models furthermore reveal additional extrema above the lithospheric step (dark grey lines in Figs 9a, b, e and f). A gravity low of up to 45 mGal in model ***Syn-sm-PhPr*** extends over *ca.* 250 km (width at half maximum), the one of up to 30 mGal in model ***Syn-sh-PhPr*** over *ca.* 150 km (width at half maximum). Elevation highs of similar widths and amplitudes of up to 450 m are seen in both models.

These extrema result from the interplay of compositional (depleted versus fertile) and thermal effects (thick versus thin lithosphere) on the SCLM bulk density. From left to right in the synthetic models, the change of SCLM composition leads first to a decrease in mass and increase in buoyancy, then the deepening of the LAB leads to a respective mass increase and buoyancy decrease. The width of the lithospheric step mainly controls the width of these extrema and, to a lesser degree, their amplitude. Different boundaries between the mantle types, which have been observed with seismic methods (e.g. Babuška & Plomerová 2006), have been tested. A very abrupt as well as a very gradual change in composition and

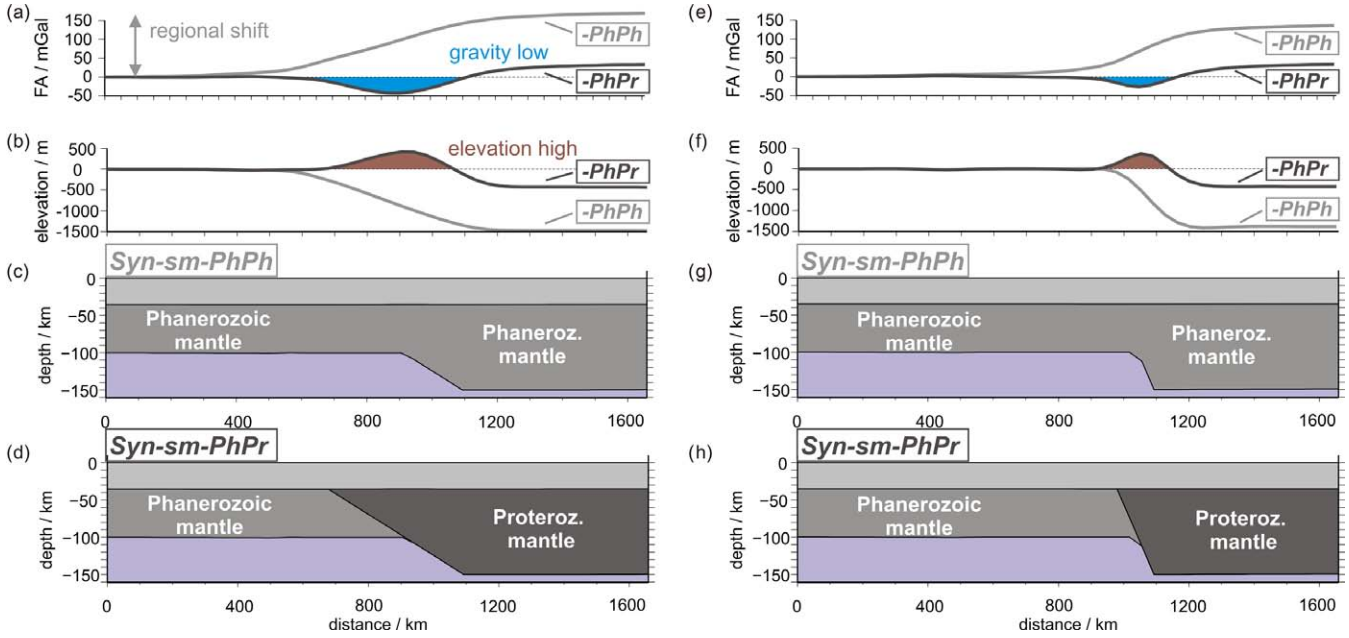

Figure 9. Left-hand side: (a, b) results and (c, d) design of synthetic models ***Syn-sm-PhPh*** and ***Syn-sm-PhPr*** with smooth lithospheric step. Right-hand side: (e, f) results and (g, h) design of synthetic models ***Syn-sh-PhPh*** and ***Syn-sh-PhPr*** with sharp lithospheric step.

thickness are expected to result in very small or no extrema. The geometry used in models ***Syn-sm-PhPr*** and ***Syn-sh-PhPr*** likely yield maximum values for the gravity low and elevation high.

Implications for Fennoscandia

The models shown here have demonstrated that adjoining lithospheres of different composition and thickness not only lead to different seismic velocities across the lateral transition zone but potentially also to gravity lows and topographic highs that trace it. The velocity differences have been well documented in southern Norway and Sweden (Maupin 2011; Medhus *et al.* 2012; Maupin *et al.* 2013), and we suggest here that further evidence for SCLM juxtaposition can be found in the remaining domains of western Fennoscandia.

The long gravity low and topographic high that extend from southern to northern Norway have commonly been separated into the regions of the southern and northern Scandes (Fig. 1a). When considering the different tectonothermal domains of Fennoscandia, in particular the western edge of the Svecofennian domain and the location of the TIB as interpreted from magnetic anomalies (Olesen *et al.* 2010), both gravity and elevation anomalies can be interpreted as forming a long, extended belt to the east in contrast to the more rounded shape of the high topography of southern Norway (Figs 10a and b). The topography in the eastern belt is especially low in the region of the Oslo Graben as well as in Mid-Norway. The regions of highest topography and lowest gravity lie in northern Norway; they overlap but do not exactly coincide. We have not yet extended our models to the north, but like to suggest here that the high topography of central and northern Norway may mark adjoining domains of different lithospheric mantles, which, among other things, would contribute to the isostatic support of the high topography. This implies that the edge of a thick, cold cratonic lithosphere would currently be located in the vicinity of the northern Norwegian margin. If adjoining mantle types results in elevated topography, it implies that this topography could have been created at the time the mantles were juxtaposed. It is challenging to argue either for or against this statement, because a palaeotopography of the order of a few hundred metres is difficult to detect. However, it is commonly assumed that the northern Norwegian mountains experience significant uplift long after the Palaeocene rifting (e.g. Doré *et al.* 2002; Anell *et al.* 2009), and we therefore do not think that the much older mantle structures discussed in this paper are directly contributing to this uplift.

The absence of high topography towards the Oslo Rift, where the lithospheric step is nevertheless best documented, may be a result of the abruptness of the SCLM changes (both thermal and compositional) as well as of the later rifting processes, responsible for the associated thinning of the crust and SCLM.

The possible juxtaposition of different SCLM in Fennoscandia raises the interesting question whether the Atlantic break-up defined this cratonic edge or whether the cratonic edge defined the position of the margin (and possibly of the earlier tectonic events such as the

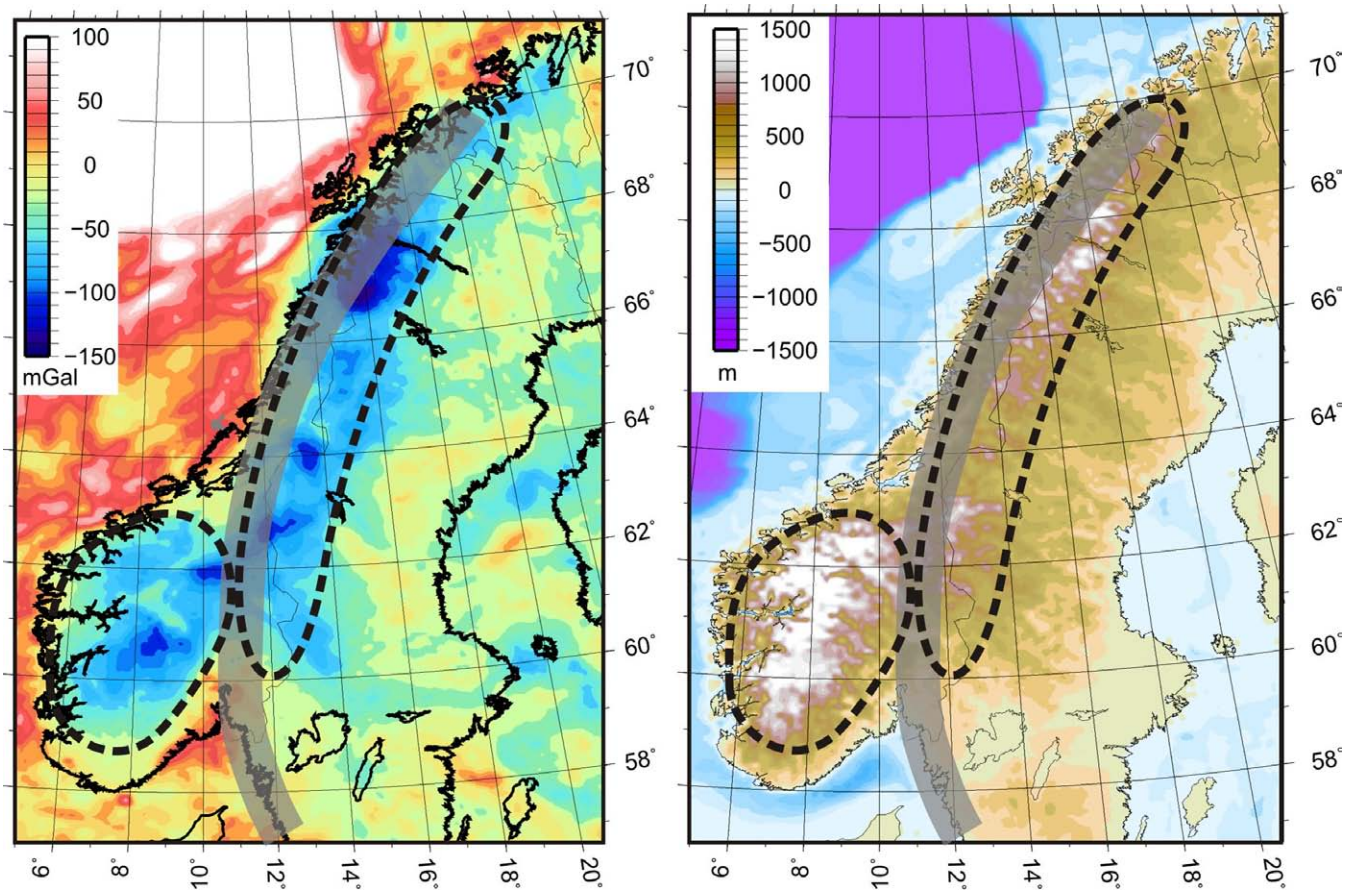

Figure 10. Proposed division of gravity anomalies and topographic structures shown on (a) Bouguer gravity map and (b) topography from southwestern Fennoscandia. The grey line indicates the edge of the Svecofennian domain and largely coincides with the elongate region of high topography and low gravity. The round region of high topography and low gravity coincides with the Sveconorwegian domain.

Caledonian orogeny). These are questions that still remain unanswered and call for further investigations.

5 CONCLUSIONS

We have performed integrated geophysical-petrological modelling of the southwestern Fennoscandian lithospheric structure testing different SCLM thicknesses and bulk compositions against observed seismic velocities, gravity anomalies and topography. It is confirmed that the high topography can be isostatically compensated in absence of a crustal root by considering lateral changes in the lower crustal structure and lithosphere thickness. A step-like increase in lithosphere thickness from southern Norway towards Sweden is inferred from the observed seismic velocities. This is accompanied by a change towards a more depleted mantle composition, which is required by the gravity field and isostatic compensation. This lateral transition zone roughly follows the edge of the Svecofennian domain in southwestern Fennoscandia, separating Meso- to Neo-Proterozoic and Palaeo-Proterozoic tectonothermal domains. We propose that this edge of the Baltic craton is a long-lived feature that has been involved and perhaps been guiding multiple subsequent tectonic events. A lateral transition between Phanerozoic-type and Proterozoic-type SCLM may result in a topographic high and a gravity low. We hypothesize that these are effects similar to those observed along a north–south axis along the Norwegian-Swedish border, marking the edge of the Fennoscandian domain.

ACKNOWLEDGEMENTS

This work was conducted in the framework of the TopoScandia-Deep project, which is part of the TOPO-EUROPE EUROCORES programme of the European Science Foundation. Additional support was given by the Norwegian Research Council. We like to thank Valerie Maupin, Tim Redfield, Marianne Lanzky Kolstrup and Christophe Pascal for valuable discussions. Furthermore, we appreciate the helpful comments of the reviewers, which led to significant improvements of this manuscript.

REFERENCES

Afonso, J.C., Ranalli, G. & Fernàndez, M., 2005. Thermal expansivity and elastic properties of the lithospheric mantle: results from mineral physics of composites, *Phys. Earth planet. Inter.*, **149**(3-4), 279–306.

Afonso, J.C., Fernàndez, M., Ranalli, G., Griffin, W.L. & Connolly, J.A.D., 2008. Integrated geophysical-petrological modeling of the lithosphere and sublithospheric upper mantle: methodology and applications, *Geochem. Geophys. Geosyst.*, **9**(5), doi:10.1029/2007GC001834.

Åhäll, K.-I. & Larson, S.Å., 2000. Growth-related 1.85-1.55 Ga magmatism in the Baltic Shield; a review addressing the tectonic characteristics of Svecofennian, TIB 1-related, and Gothian events, *GFF*, **122**(2), 193–206.

Andersen, O.B., Knudsen, P. & Berry, P.A., 2010. The DNSC08GRA global marine gravity field from double retracked satellite altimetry, *J. Geod.*, **84,** 191–199.

Anderson, U., 1997. Petrogenesis of some Proterozoic granitoid suites and associated basic rocks in Sweden (geochemistry and isotope geology), Rapporter och Meddelanden – Sveriges Geologiska Undersökning, **91**.

Andersson, J., Möller, C. & Johansson, L., 2002. Zircon geochronology of migmatite gneisses along the Mylonite Zone (S Sweden): a major Sveconorwegian terrane boundary in the Baltic Shield, *Precambrian Res.*, **114**(1-2), 121–147.

Anell, I., Thybo, H. & Artemieva, I., 2009. Cenozoic uplift and subsidence in the North Atlantic region: geological evidence revisited, *Tectonophysics*, **474**(1-2), 78–105.

Arlitt, R., Kissling, E. & Ansorge, J., 1999. Three-dimensional crustal structure beneath the TOR array and effects on teleseismic wavefronts, *Tectonophysics*, **314**(1-3), 309–319.

Artemieva, I.M., Thybo, H. & Kaban, M.K., 2006. Deep Europe today: Geophysical synthesis of the upper mantle structure and lithospheric processes over 3.5 Ga, *Geol. Soc., Lond., Memoirs*, **32**(1), 11–41.

Babuška, V. & Plomerová, J., 2004. The Sorgenfrei-Tornquist Zone as the mantle edge of Baltica lithosphere: new evidence from three-dimensional seismic anisotropy, *Terra Nova*, **16**(5), 243–249.

Babuška, V. & Plomerová, J., 2006. European mantle lithosphere assembled from rigid microplates with inherited seismic anisotropy, *Phys. Earth planet. Inter.*, **158**(2-4), 264–280.

Balling, N., 1980. The land uplift in Fennoscandia, gravity field anomalies and isostasy, in *Earth Rheology, Isostasy and Eustacy, Conference Proceedings of Earth Rheology and Late Cenozoic Isostatic Movements*, Stockholm, Sweden, Vol. 32, pp. 297–321, ed. Moerner, N., John Wiley and Sons, Chichester, United Kingdom.

Bannister, S., Ruud, B. & Husebye, E., 1991. Tomographic estimates of sub-Moho seismic velocities in Fennoscandia and structural implications, *Tectonophysics*, **189**(1-4), 37–53.

Beyer, E.E., Brueckner, H.K., Griffin, W.L., O'Reilly, S.Y. & Graham, S., 2004. Archean mantle fragments in Proterozoic crust, Western Gneiss Region, Norway, *Geology*, **32**(7), 609–612.

Bingen, B. *et al.*, 2005. Timing of continental building in the Sveconorwegian orogen, SW Scandinavia, *Norwegian J. Geol.*, **85,** 87–116.

Bingen, B., Nordgulen, Ø. & Viola, G., 2008. A four-phase model for the Sveconorwegian orogeny, SW Scandinavia, *Norwegian J. Geol.*, **88,** 43–72.

Calcagnile, G., 1982. The lithosphere-asthenosphere system in Fennoscandia, *Tectonophysics*, **90**(1-2), 19–35.

Connolly, J., 2005. Computation of phase equilibria by linear programming: a tool for geodynamic modeling and its application to subduction zone decarbonation, *Earth planet. Sci. Lett.*, **236**(1-2), 524–541.

Connolly, J. & Kerrick, D., 2002. Metamorphic controls on seismic velocity of subducted oceanic crust at 100-250 km depth, *Earth planet. Sci. Lett.*, **204**(1-2), 61–74.

Cook, F.A., White, D.J., Jones, A.G., Eaton, D.W., Hall, J. & Clowes, R.M., 2010. How the crust meets the mantle: lithoprobe perspectives on the Mohorovicic discontinuity and crust-mantle transition, *Can. J. Earth Sci.*, **47**(4), 315–351.

Cotte, N., Pedersen, H. & TOR Working Group, 2002. Sharp contrast in lithospheric structure across the Sorgenfrei-Tornquist Zone as inferred by Rayleigh wave analysis of TOR1 project data, *Tectonophysics*, **360**(1-4), 75–88.

Divins, D., 2012. NGDC total sediment thickness of the World's oceans and marginal seas, Available at: http://www.ngdc.noaa.gov/mgg/sedthick/sedthick.html. Last accessed March 2012.

Djomani, Y.H.P., O'Reilly, S.Y., Griffin, W. & Morgan, P., 2001. The density structure of subcontinental lithosphere through time, *Earth planet. Sci. Lett.*, **184**(3-4), 605–621.

Doré, A.G., Cartwright, J.A., Stoker, M.S., Turner, J.P. & White, N.J., 2002. Exhumation of the North Atlantic margin: introduction and background, *Geol. Soc., Lond., Special Publ.*, **196**(1), 1–12.

Eaton, D.W., Darbyshire, F., Evans, R.L., Grütter, H., Jones, A.G. & Yuan, X., 2009. The elusive lithosphere-asthenosphere boundary (LAB) beneath cratons, *Lithos*, **109**(1-2), 1–22.

Ebbing, J., 2007. Isostatic density modelling explains the missing root of the Scandes, *Norwegian J. Geol.*, **87,** 13–20.

Ebbing, J. & Olesen, O., 2010. New compilation of top basement and basement thickness for the Norwegian continental shelf reveals the segmentation of the passive margin system, *Geol. Soc., Lond., Petrol. Geol. Conf. Ser.*, **7,** 885–897.

Ebbing, J., England, R., Korja, T., Lauritsen, T., Olesen, O., Stratford, W. & Weidle, C., 2012. Structure of the Scandes lithosphere from surface to depth, *Tectonophysics*, **536-537,** doi:10.1016/j.tecto.2012.02.016.

Eken, T., Shomali, Z.H., Roberts, R., Hieronymus, C.F. & Bodvarsson, R., 2008. S and P velocity heterogeneities within the upper mantle below the Baltic shield, *Tectonophysics*, **462**(1-4), 109–124.

England, R.W. & Ebbing, J., 2012. Crustal structure of central Norway and Sweden from integrated modelling of teleseismic receiver functions and the gravity anomaly, *Geophys. J. Int.*, **191**(1), 1–11.

Esedo, R., van Wijk, J., Coblentz, D. & Meyer, R., 2012. Uplift prior to continental breakup: indication for removal of mantle lithosphere?, *Geosphere*, **8**(5), 1078–1085.

Færseth, R. & Lien, T., 2002. Cretaceous evolution in the Norwegian Sea—a period characterized by tectonic quiescence, *Mar. Petrol. Geol.*, **19**(8), 1005–1027.

Fischer, K.M., Ford, H.A., Abt, D.L. & Rychert, C.A., 2010. The lithosphere-asthenosphere boundary, *Ann. Rev. Earth planet. Sci.*, **38**(1), 551–575.

Fullea, J., 2008. Development of numerical methods to determine the lithospheric structure combining geopotential, lithostatic and heat transport equations. application to the Gibraltar arc system, *PhD thesis*, Univ. de Barcelona, Barcelona, Spain.

Fullea, J., Afonso, J.C., Connolly, J.A.D., Fernàndez, M., García-Castellanos, D. & Zeyen, H., 2009. LitMod3D: an interactive 3-D software to model the thermal, compositional, density, seismological, and rheological structure of the lithosphere and sublithospheric upper mantle, *Geochem. Geophys. Geosyst.*, **10**(8), doi:10.1029/2009GC002391.

Gaal, G. & Gorbatschev, R., 1987. An outline of the Precambrian evolution of the Baltic Shield, *Precambrian Res.*, **35,** 15–52.

Garcia-Castellanos, D., 2002. Interplay between lithospheric flexure and river transport in foreland basins, *Basin Res.*, **14**(2), 89–104.

Gorbatchev, R., 2004. The Transscandinavian Igneous Belt—introduction and background, in *The Transscandinavian Igneous Belt (TIB) in Sweden: A review of its character and evolution, Geological Survey of Finland, Special Paper,* Vol. 37, pp. 9–15, eds Högdahl, K., Andersson, U. & Eklund, O., Geological Survey of Finland.

Gorbatschev, R. & Bogdanova, S., 1993. Frontiers in the Baltic Shield, *Precambrian Res.*, **64,** 3–21.

Grad, M., Tiira, T. & Group, E.W., 2009. The Moho depth map of the European plate, *Geophys. J. Int.*, **176**(1), 279–292.

Guggisberg, B., Kaminski, W. & Prodehl, C., 1991. Crustal structure of the Fennoscandian Shield: a traveltime interpretation of the long-range FENNOLORA seismic refraction profile, *Tectonophysics*, **195**(2-4), 105–137, doi:10.1016/0040-1951(91)90208-A.

Hieronymus, C.F. & Goes, S., 2010. Complex cratonic seismic structure from thermal models of the lithosphere: effects of variations in deep radiogenic heating, *Geophys. J. Int.*, **180**(3), 999–1012.

Hieronymus, C.F., Shomali, Z.H. & Pedersen, L.B., 2007. A dynamical model for generating sharp seismic velocity contrasts underneath continents: Application to the Sorgenfrei-Tornquist Zone, *Earth planet. Sci. Lett.*, **262**(1-2), 77–91.

Hofmeister, A.M., 1999. Mantle values of thermal conductivity and the geotherm from phonon lifetimes, *Science*, **283**(5408), 1699–1706.

Husebye, H., Hovland, J., Christoffersson, A., Åström, K., Slunga, R. & Lund, C.-E., 1986. Tomographical mapping of the lithosphere and asthenosphere beneath southern Scandinavia and adjacent areas, *Tectonophysics*, **128,** 229–250.

Japsen, P., Green, P.F., Nielsen, L.H., Rasmussen, E.S. & Bidstrup, T., 2007. Mesozoic-Cenozoic exhumation events in the eastern North Sea Basin: a multi-disciplinary study based on palaeothermal, palaeoburial, stratigraphic and seismic data, *Basin Res.*, **19**(4), 451–490.

Japsen, P., Chalmers, J.A., Green, P.F. & Bonow, J.M., 2012. Elevated, passive continental margins: not rift shoulders, but expressions of episodic, post-rift burial and exhumation, *Global planet. Change*, **90-91**(0), 73–86.

Jones, A.G., Plomerová, J., Korja, T., Sodoudi, F. & Spakman, W., 2010. Europe from the bottom up: a statistical examination of the central and northern european lithosphere-asthenosphere boundary from comparing seismological and electromagnetic observations, *Lithos*, **120**(1-2), 14–29.

Karato, S., 1993. Importance of anelasticity in the interpretation of seismic tomography, *Geophys. Res. Lett.*, **20**(15), 1623–1626.

Karato, S. & Jung, H., 1998. Water, partial melting and the origin of the seismic low velocity and high attenuation zone in the upper mantle, *Earth planet. Sci. Lett.*, **157**(3-4), 193–207.

Kinck, J., Husebye, E. & Larsson, F., 1993. The Moho depth distribution in Fennoscandia and the regional tectonic evolution from Archean to Permian times, *Precambrian Res.*, **64**(1-4), 23–51.

Klemme, S., 2004. The influence of Cr on the garnet-spinel transition in the Earth's mantle: experiments in the system MgO-Cr_2O_3-SiO_2 and thermodynamic modelling, *Lithos*, **77**(1-4), 639–646.

Kolstrup, M.L., Pascal, C. & Maupin, V., 2012. What compensates the topography of southern Norway? Insights from thermo-isostatic modeling, *J. Geodyn.*, **61**(0), 105–119.

Korja, A., Korja, T., Luosto, U. & Heikkinen, P., 1993. Seismic and geoelectric evidence for collisional and extensional events in the Fennoscandian Shield implications for Precambrian crustal evolution, *Tectonophysics*, **219**(1-3), 129–152.

Korja, T., Smirnov, M., Pedersen, L. & Gharibi, M., 2008. Structure of the central Scandinavian Caledonides and the underlying Precambrian basement, new constraints from magnetotellurics, *Geophys. J. Int.*, **175**(1), 55–69.

Korsman, K., Korja, T., Pajunen, M. & Virransalo, P., 1999. The GGT/SVEKA transect: structure and evolution of the continental crust in the Paleoproterozoic Svecofennian orogen in Finland, *Int. Geol. Rev.*, **41**(4), 287–333.

Lahtinen, R., Korja, A. & Nironen, M., 2005. Palaeoproterozoic tectonic evolution of the Fennoscandian Shield, in *Precambrian Geology of Finland—Key to the Evolution of the Fennoscandian Shield, Developments in Precambrian Geology,* Vol. 14, pp. 481–531, eds Lehtinen, P.N.M. & Rämö, O., Elsevier, Amsterdam, The Netherlands.

Lahtinen, R., Korja, A., Nironen, M. & Heikkinen, P., 2009. Palaeoproterozoic accretionary processes in Fennoscandia, *Geol. Soc., Lond., Special Publ.*, **318**(1), 237–256.

Larson, S. & Berglund, J., 1992. A chronological subdivision of the Transscandinavian Igneous Belt—three magmatic episodes?, *Geologiska Föreningen i Stockholm Förhandlingar,* **114**(4), 459–461.

Lebedev, S., Boonen, J. & Trampert, J., 2009. Seismic structure of Precambrian lithosphere: new constraints from broad-band surface-wave dispersion, *Lithos*, **109**(1-2), 96–111.

Lidmar-Bergström, K., Ollier, C. & Sulebak, J., 2000. Landforms and uplift history of southern Norway, *Global planet. Change*, **24**(3-4), 211–231.

Lidmar-Bergström, K., Näslund, J.-O., Ebert, K., Neubeck, T. & Bonow, J., 2007. Cenozoic landscape development on the passive margin of northern Scandinavia, *Norwegian J. Geol.*, **87,** 181–196.

Lund, C.-E., 1987. Crustal structure along the northern 'Fennolora' profile, *Precambrian Res.*, **35**(0), 195–206.

Maupin, V., 2011. Upper-mantle structure in southern Norway from beamforming of Rayleigh wave data presenting multipathing, *Geophys. J. Int.*, **185**(2), 985–1002.

Maupin, V. *et al.*, 2013. The deep structure of the Scandes and its relation to tectonic history and present-day topography, *Tectonophysics*, doi:10.1016/j.tecto.2013.03.010.

Medhus, A., Balling, N., Jacobsen, B., Kind, R. & England, R., 2009. Deep structural differences in southwestern Scandinavia revealed by P-wave travel time residuals, *Norwegian J. Geol.*, **89,** 203–214.

Medhus, A.B., Balling, N., Jacobsen, B.H., Weidle, C., England, R.W., Kind, R., Thybo, H. & Voss, P., 2012. Upper-mantle structure beneath the Southern Scandes Mountains and the Northern Tornquist Zone revealed by P-wave traveltime tomography, *Geophys. J. Int.*, **189**(3), 1315–1334.

Minster, B. & Anderson, D.L., 1981. A model of dislocation-controlled rheology for the mantle, *Phil. Trans. R. Soc.*, **A**(299), 319–356.

Nagy, D., Papp, G. & Benedek, J., 2000. The gravitational potential and its derivatives for the prism, *J. Geod.*, **74,** 552–560.

Neumann, E.-R., Olsen, K., Baldridge, W. & Sundvoll, B., 1992. The Oslo Rift: a review, *Tectonophysics*, **208**(1-3), 1–18.

Nielsen, S.B. *et al.*, 2009. The evolution of western Scandinavian topography: a review of Neogene uplift versus the ICE (isostasy-climate-erosion) hypothesis, *J. Geodyn.*, **47**(2-3), 72–95.

Olesen, O. *et al.*, 2007. KONTIKI Final Report, CONTInental Crust and Heat Generation In 3D., NGU Report 2007.042, NGU, Geological Survey of Norway.

Olesen, O. *et al.*, 2010. New aeromagnetic and gravity compilations from Norway and adjacent areas: methods and applications, *Geol. Soc., Lond., Petrol. Geol. Conf. Ser.,* **7,** 559–586.

Osmundsen, P., Sommaruga, A., Skilbrei, J. & Olesen, O., 2002. Deep structure of the mid-Norway rifted margin, *Norwegian J. Geol.,* **82,** 205–224.

Osmundsen, P.T. & Ebbing, J., 2008. Styles of extension offshore mid-Norway and implications for mechanisms of crustal thinning at passive margins, *Tectonics*, **27**(TC6016), doi:10.1029/2007TC002242.

Osmundsen, P.T. & Redfield, T.F., 2011. Crustal taper and topography at passive continental margins, *Terra Nova*, **23**(6), 349–361.

Pascal, C. & Olesen, O., 2009. Are the Norwegian mountains compensated by a mantle thermal anomaly at depth?, *Tectonophysics*, **475**(1), 160–168.

Pascal, C., van Wijk, J.W., Cloetingh, S.A.P.L. & Davies, G.R., 2002. Effect of lithosphere thickness heterogeneities in controlling rift localization: numerical modeling of the Oslo Graben, *Geophys. Res. Lett.*, **29**(9), 69-1–69-4.

Pascal, C., Cloetingh, S.A.P.L. & Davies, G.R., 2004. Asymmetric lithosphere as the cause of rifting and magmatism in the Permo-Carboniferous Oslo Graben, *Geol. Soc., Lond., Special Publ.*, **223**(1), 139–156.

Patchett, P., Todt, W. & Gorbatschev, R., 1987. Origin of continental crust of 1.9-1.7 Ga age; Nd isotopes in the Svecofennian orogenic terrains of Sweden, *Precambrian Res.*, **35,** 145–160.

Pavlis, N., Holmes, S., Kenyon, S. & Factor, J., 2008. An Earth gravitational model to degree 2160: EGM 2008, in *Proceedings of the GRACE Science Applications, Session G3*, EGU, Vienna.

Pedersen, H., Fishwick, S. & Snyder, D., 2009. A comparison of cratonic roots through consistent analysis of seismic surface waves, *Lithos*, **109**(1-2), 81–95.

Petit, C. & Déverchère, J., 2006. Structure and evolution of the Baikal rift: a synthesis, *Geochem. Geophys. Geosyst.*, **7**(Q11016), doi:10.1029/2006GC001265.

Pilidou, S., Priestley, K., Gudmundsson, O. & Debayle, E., 2004. Upper mantle S-wave speed heterogeneity and anisotropy beneath the North Atlantic from regional surface wave tomography: the Iceland and Azores plumes, *Geophys. J. Int.*, **159**(3), 1057–1076.

Plomerová, J., Arvidsson, R., Babuška, V., Granet, M., Kulhánek, O., Poupinet, G. & Šílený, J., 2001. An array study of lithospheric structure across the Protogine zone, Värmland, south-central Sweden—signs of a paleocontinental collision, *Tectonophysics*, **332**(1-2), 1–21.

Plomerová, J., Babuška, V., Vecsey, L. & Kouba, D., 2002. Seismic anisotropy of the lithosphere around the Trans-European Suture Zone (TESZ) based on teleseismic body-wave data of the TOR experiment, *Tectonophysics*, **360**(1-4), 89–114.

Plomerová, J., Babuška, V., Kozlovskaya, E., Vecsey, L. & Hyvönen, L., 2008. Seismic anisotropy—a key to resolve fabrics of mantle lithosphere of Fennoscandia, *Tectonophysics*, **462**(1-4), 125–136.

Popp, T. & Kern, H., 1993. Thermal dehydration reactions characterised by combined measurements of electrical conductivity and elastic wave velocities, *Earth planet. Sci. Lett.*, **120**(1-2), 43–57.

Redfield, T. & Osmundsen, P., 2012. The long-term topographic response of a continent adjacent to a hyperextended margin: a case study from Scandinavia, *Geol. Soc. Am. Bull.*, doi:10.1130/B30691.1.

Redfield, T., Braathen, A., Gabrielsen, R., Osmundsen, P., Torsvik, T. & Andriessen, P., 2005. Late Mesozoic to Early Cenozoic components of vertical separation across the Møre-Trøndelag Fault complex, Norway, *Tectonophysics*, **395**(3-4), 233–249.

Rohrman, M. & van der Beek, P., 1996. Cenozoic postrift domal uplift of North Atlantic margins: an asthenospheric diapirism model, *Geology*, **24**(10), 901–904.

Schivardi, R. & Morelli, A., 2009. Surface wave tomography in the European and Mediterranean region, *Geophys. J. Int.*, **177**(3), 1050–1066.

Schubert, G., Turcotte, D.L. & Olson, P., 2001. *Mantle Convection in the Earth and Planets*, 940 pp., Cambridge University Press, Cambridge, Cambridge, United Kingdom (GBR).

Shomali, Z.H., Roberts, R.G. & the TOR Working Group, 2002. Non-linear body wave teleseismic tomography along the TOR array, *Geophys. J. Int.*, **148**(3), 562–574.

Shomali, Z.H., Roberts, R.G. & Pedersen, L.B., 2006. Lithospheric structure of the Tornquist Zone resolved by nonlinear P and S teleseismic tomography along the TOR array, *Tectonophysics*, **416**(1-4), 133–149.

Slagstad, T., 2008. Radiogenic heat production of Archaean to Permian geological provinces in Norway, *Norwegian J. Geol.*, **88,** 149–166.

Slagstad, T., Balling, N., Elvebakk, H., Midttømme, K., Olesen, O., Olsen, L. & Pascal, C., 2009. Heat-flow measurements in Late Palaeoproterozoic to Permian geological provinces in south and central Norway and a new heat-flow map of Fennoscandia and the Norwegian-Greenland Sea, *Tectonophysics*, **473**(3-4), 341–361.

Slagstad, T., Roberts, N.M.W., Marker, M., Røhr, T.S. & Schiellerup, H., 2013. A non-collisional, accretionary Sveconorwegian orogen, *Terra Nova*, **25**(1), 30–37.

Smith, W.H.F. & Sandwell, D.T., 1997. Global sea floor topography from satellite altimetry and ship depth soundings, *Science*, **277**(5334), 1956–1962.

Solomatov, V.S. & Moresi, L.N., 2000. Scaling of time-dependent stagnant lid convection; application to small-scale convection on Earth and other terrestrial planets, *J. geophys. Res.*, **105**(B9), 21 795–21 817.

Stixrude, L. & Lithgow-Bertelloni, C., 2005. Mineralogy and elasticity of the oceanic upper mantle: origin of the low-velocity zone, *J. geophys. Res.*, **110**(B03204), doi:10.1029/2004JB002965.

Stratford, W., Thybo, H., Faleide, J.I., Olesen, O. & Tryggvason, A., 2009. New Moho map for onshore southern Norway, *Geophys. J. Int.*, **178**(3), 1755–1765.

Svenningsen, L., Balling, N., Jacobsen, B.H., Kind, R., Wylegalla, K. & Schweitzer, J., 2007. Crustal root beneath the highlands of southern Norway resolved by teleseismic receiver functions, *Geophys. J. Int.*, **170**(3), 1129–1138.

Wawerzinek, B., Ritter, J. & Roy, C., 2013. New constraints on the 3D shear wave velocity structure of the upper mantle underneath southern Scandinavia revealed from non-linear tomography, *Tectonophysics*, doi:10.1016/j.tecto.2012.12.033.

Weidle, C. & Maupin, V., 2008. An upper-mantle S-wave velocity model for northern Europe from Love and Rayleigh group velocities, *Geophys. J. Int.*, **175**(3), 1154–1168.

Yuan, H. & Romanowicz, B., 2010. Lithospheric layering in the North American Craton, *Nature (London)*, **466**(7310), 1063–1068.

Zaranek, S.E. & Parmentier, E., 2004. The onset of convection in fluids with strongly temperature-dependent viscosity cooled from above with implications for planetary lithospheres, *Earth planet. Sci. Lett.*, **224**(3-4), 371–386.